Mapping the Excited States of Single Hexa-*peri*-benzocoronene Oligomers

We-Hyo Soe,[†,*] Hon Seng Wong,[†] Carlos Manzano,[†] Maricarmen Grisolia,[‡] Mohamed Hliwa,[‡,§] Xinliang Feng,[⊥] Klaus Müllen,[⊥] and Christian Joachim[†,‡]

[†]IMRE, A*STAR (Agency for Science, Technology and Research), 3 Research Link, 117602, Singapore, [‡]GNS-CEMES, CNRS, 29 rue J. Marvig, 31055 Toulouse Cedex, France, [§]Faculté des Sciences Ben M'Sik, Université Hassan II-Mohammedia, B.P. 7955 Sidi Othman, Casablanca, Morroco, and [⊥]Max Planck Institute for Polymer Research, Ackermannweg 10, D-55128 Mainz, Germany

ABSTRACT

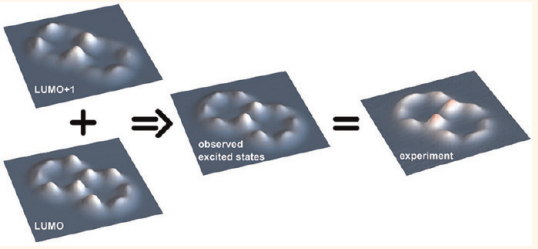

Electronic states of a molecule are usually analyzed *via* their decomposition in linear superposition of multielectronic Slater determinants built up from monoelectronics molecular orbitals. It is generally believed that a scanning tunneling microscope (STM) is able to map those molecular orbitals. Using a low-temperature ultrahigh vacuum (LT-UHV) STM, the d*I*/d*V* conductance maps of large single hexabenzocoronene (HBC) monomer, dimer, trimer, and tetramer molecules were recorded. We demonstrate that the attribution of a tunnel electronic resonance to a peculiar π molecular orbital of the molecule (or σ intermonomer chemical bond) in the STM junction is inappropriate. With an STM weak-measurement-like procedure, a d*I*/d*V* resonance results from the conductance contribution of many molecular states whose superposition makes it difficult to reconstruct an apparent molecular orbital electron probability density map.

KEYWORDS: quantum chemistry · π interactions · scanning tunneling spectroscopy · surface science

The electronic quantum states $|\psi_n\rangle$ of an *N*-electron molecule are usually expressed using monoelectronic molecular orbitals leading to a reduced one-electron $\rho_n(r)$ probability density distribution to describe the expansion of the corresponding molecule electronic cloud in space.[1] Among them, the $\rho_0(r)$ reduced density map of the $|S_0\rangle$ ground state of closed shell molecules such as phthalocyanine or pentacene has been used to interpret field emission microscope (FEM),[2] transmission electron microscope (TEM),[3] reconstructed inverse photoemission (IPE),[4] STM,[5−7] and noncontact atomic force microscope (NC-AFM)[8,9] images. It is generally assumed that at least the $|S_0\rangle$ secular decomposition on a set of Slater determinants built up from those monoelectronic molecular orbitals is not modified by the transfer function of the FEM, TEM, IPE, STM, or NC-AFM instruments.

With an almost uniform local density of states (LDOS), metallic surface, and with a physisorbed molecule, the d*I*/d*V* spectrum of an STM molecular junction is characterized by electronic resonances, indicating the energy position of the molecule $|\psi_n\rangle$ relative to the E_F bulk metal Fermi level.[6,7] Scanning using a constant current d*I*/d*V* mode maps the junction electronic conductance exactly at the resonant energy selected by the bias voltage *V*. In this mode, the STM feedback loop can maintain a very weak electronic coupling between the tip apex and the molecule. This favors the overlap between the tip apex end states and very specific molecular orbitals[10] entering in the composition of the $|\psi_n\rangle$ *N*-electron Slater determinants. At a given location on the molecule, the tip apex is generally coupled to more than one $|\psi_n\rangle$. Only in very specific cases, the contribution to the conductance of those $|\psi_n\rangle$ located in energy within the stable voltage-biased window of the junction will reconstruct a given molecular orbital electron probability distribution.[7]

We demonstrate in this paper how the quantum information about the intermonomer chemical bond(s) of large hexabenzocoronene dimers, trimers, and tetramers (HBC(*n*)) molecules adsorbed on a Au(111) surface can be traced in real space. HBC is known as a super benzene molecule[11] where the ground and first excited states are easily decomposed on Slater determinants built up using π molecular orbitals in an $\sigma-\pi$ separation model. The Au(111) surface was selected because this HBC(*n*) series physisorbed on Au(111), an essential prerequisite to preserve the $\rho_n(r)$ native real space spatial extension.[6,7]

* Address correspondence to wh-soe@imre.a-star.edu.sg.

Received for review January 9, 2012 and accepted March 27, 2012.

Published online March 27, 2012
10.1021/nn300110k

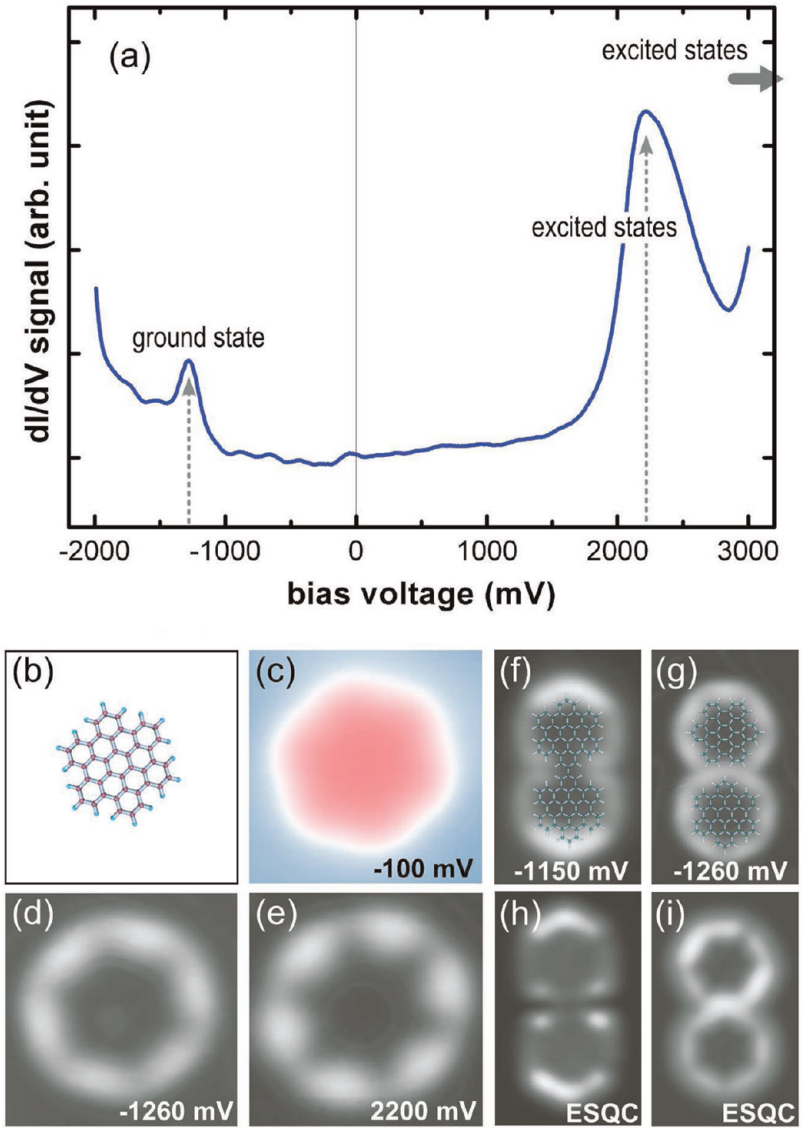

Figure 1. Scanning tunneling spectroscopic data of single HBC molecule. (a) d*I*/d*V* spectrum for a HBC molecule absorbed on Au(111) surface. (b) Ball-and-stick model of HBC molecule. (c) STM topographic image of a single HBC at a nonresonant energy and, (d,e) its d*I*/d*V* differential conductance maps taken at the resonant state energies at both polarities. (f) For comparison, the d*I*/d*V* map of true HBC(2) dimer at the first energy peak in the negative side of the spectra shown in Figure 2a, and (g) d*I*/d*V* map for a vdW HBC dimer and (h,i) their corresponding calculated ESQC images. Ball-and-stick molecule models are also superimposed in panels f and g to show the distance between each HBC monomer forming the dimers, and their center-to-center distances are 1.28 and 1.44 nm, respectively. Image sizes are 2.5 nm × 2.5 nm for b−e and 2.6 nm × 3.6 nm for f−i.

RESULTS AND DISCUSSION

We have first prepared a sub-monolayer of HBC molecules on a Au(111) surface with no postdeposition annealing. The LT-UHV STM images show individual HBC molecules adsorbed at both step edges and on the Au terraces. Only single isolated HBC molecules were observed. The low bias voltage STM constant current image (Figure 1c) shows a single HBC molecule adsorbed on the Au(111) surface with no internal contrast. Due to its intrinsic symmetry and in order to maximize its van der Waals (vdW) interaction with the Au(111) surface, HBC adopts a flat-lying adsorption geometry. The d*I*/d*V* spectrum recorded at the periphery of an isolated HBC (Figure 1a) picks up a first electronic resonance at −1.30 V below and a second one at +2.20 V above E_F. A third resonance was identified slightly beyond 3.0 V, but at these voltages, the molecules are not stable enough to perform d*I*/d*V* imaging. The d*I*/d*V* STM maps were recorded at −1.26 and +2.20 V to map the spatial variation of the electronic transparency of the molecular junction, as shown in Figure 1d,e. Both images are showing a constant electronic transparency at the center of the molecule and six bright lobes at its periphery. Those bright lobes are rotated 30° with respect to the outer HBC phenyl ring positions (see Figure 1b−e). The elastic scattering quantum chemistry (ESQC) calculations were performed under the monoelectronic level

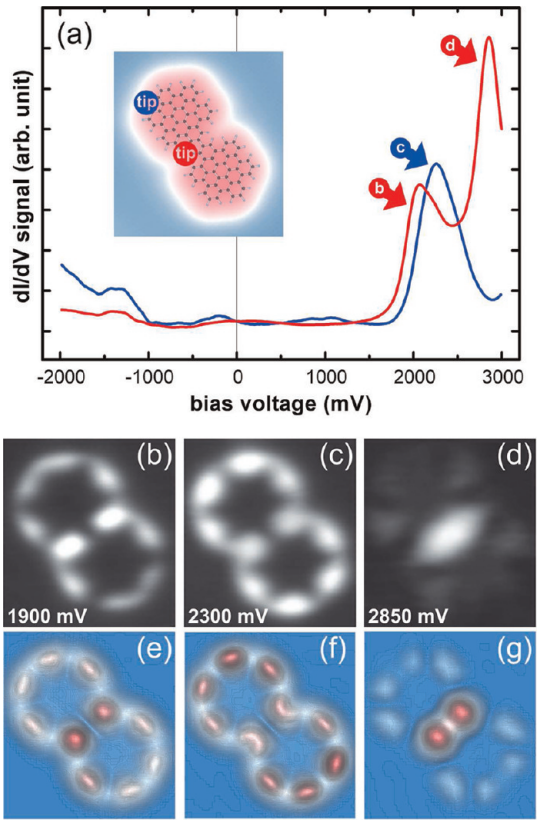

Figure 2. Scanning tunneling spectroscopic data of single HBC(2) dimer. (a) d*I*/d*V* spectra taken at the center between HBC partners (red line) and on the outer edge of the dimer (blue line). Inset shows the topographic image of a HBC(2) dimer and a superimposed ball-and-stick molecule model, the exact tip locations where each spectrum was measured are shown by the corresponding colored dots. (b−d) Experimental d*I*/d*V* maps taken at the peak positions labeled in the spectrum, and (e−g) their corresponding optimized ESQC images (see Supporting Information). All images are 3.2 nm × 3.2 nm.

approximation[12] considering only the highest occupied molecular orbital (HOMO) for −1.26 V and the first lowest unoccupied molecular orbital (LUMO) for +2.20 V. According to the Hohenberg−Kohn theorem, the ground state of an *N*-electron system can be described by a one-electron density functional.[13] Therefore, a good way to describe the −1.3 V resonance map is to build up this functional starting from the HOMO component of the A_{1g} $|S_0\rangle$ HBC ground state. The experimental and monoelectronic ESQC calculated images are in agreement as presented in Figure 1. For the +2.20 V resonance, there must be a very fast transient virtual occupation of a few of the B_{2u}, E_{1u} B_{1u}, E_{2g} ... $|\psi_m^*\rangle$ low-lying HBC electronic excited states.[14] Consequently, the d*I*/d*V* image originates mainly from six of those states with a large weight on the e_{2u} molecular orbital level (almost degenerate on the surface LUMO and LUMO+1). Therefore, the ESQC image calculated at the e_{2u} monoelectronic energy reproduces quite well the +2.20 V resonance d*I*/d*V* experimental images (see Supporting Information). Furthermore and opposite to certain organometallic molecules,[15] the electron transfer through those $|\psi_m^*\rangle$ excited states is so fast that no intramolecular conformation change can be observed.

Two HBC molecules were also manipulated and brought together by STM manipulation[16] to follow if and how the HBC electronic states of both partners could hybridize. The ground state experimental and HOMO ESQC calculated d*I*/d*V* images of the two HBCs are simply a normalized superposition of single HBC's ground state images, as presented in Figure 1g,i. Regardless the relative orientation of the two HBCs, it was not possible to form a chemical bond between the two. After assembling many different HBC vdW dimers, two intact and separated HBC molecules are always recovered again after further STM molecular manipulations.

Another sample was identically prepared, this time followed by a postannealing of the Au(111) surface at about 600 K for the HBC dehydrogenation reaction to take place.[17] The LT-UHV STM images of the surface now reveal the on-surface synthesized HBC oligomers: dimers, trimers, tetramers, and long random HBC chains appear because of the random formation of HBC mono-, di-, and triradicals during the annealing. These oligomers were STM manipulated to ascertain the formation of covalent-bonded large HBC(*n*) molecules rather than vdW complexes. Their d*I*/d*V* spectra were taken only for positive bias voltage since it was not possible to clearly resolve the d*I*/d*V* resonances below the Fermi level (see Figure 2a for $V < -1.0$ V). We attribute this to the large number of possible oxidized state resonances that cannot be nicely separated below the HBC(*n*) ground state STM electronic resonance.

At the periphery of an HBC(2) dimer, the d*I*/d*V* has only one resonance at +2.25 V. At the center, between the two HBC(2) partners of the same dimer, two pronounced resonances at +2.05 and +2.85 V are observed (Figure 2a). The corresponding d*I*/d*V* maps presented in Figure 2b−d were recorded to identify the excited states responsible for those resonances. The lower energy sets at +1.90 and +2.25 V have both the same symmetry and conductance map spatial arrangements. To record the d*I*/d*V* conductance maps of the first +2.05 V peak, a slightly lower voltage than the exact resonance value was used in order to relatively maximize the junction conductance between the two peaks. As compared with the Figure 1e d*I*/d*V* map, only the contrast of HBC(2) bond location has changed in the image, indicating the relative orientation of the two HBC moieties.

Using the PM6-CIS calculation approximation,[18] twelve $|\psi_m^*\rangle$ excited states have been identified in the +2.25 V energy range contributing to the molecular junction conductance. They are composed of mono-excited Slater determinants mainly built up by promoting one valence electron to the virtual molecular orbitals ranging from LUMO to LUMO+3. They belong to the first six LUMOs of HBC(2) issued from the

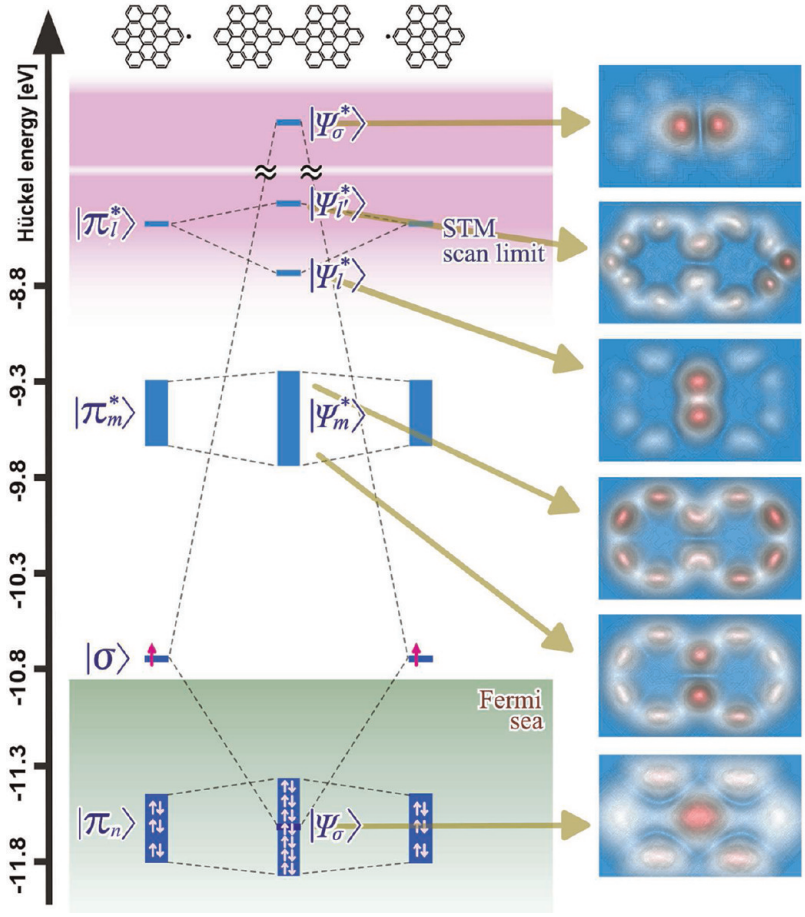

Figure 3. Schematic diagram of the molecular orbitals energy levels of HBC(2) before and after the central bond formation. The relatively scaled energy levels and widths are calculated based on the extended Hückel theory. On the right, ESQC images calculated at the selected energies indicated by arrows. The topmost $|\psi_\sigma^*\rangle$ antibonding σ state image was computed for slightly larger distance separation between the HBC partners than in HBC(2) to reduce the energy splitting effect relative to its bonding counterpart. All images are 3.4 nm $\times$ 2.4 nm.

hybridization of the first three LUMOs of each HBC fragment (see Figure 3 and Supporting Information). Each of the six corresponding ESQC calculated monoelectronic STM images match quite well the experimental Figure 2b,c d*I*/d*V* maps. For a better match with the experimental images, an optimization was performed for superposing the calculated monoelectronic images to the experimental ones, as presented in Figure 2e,f.[7] This confirms that the +2.05 and +2.25 V resonances are coming from the electronic interactions between the tip apex and those 12 states. The experimental d*I*/d*V* maps arise from the conductance tunnel paths through the molecular states selectively captured by the tip at each energy and position. A detailed analysis of those states shows that none of them is responsible for the σ chemical bonding between the two HBC moieties. The +2.25 V resonance captured away from the intermonomer bond is located at the same energy as the first positive resonance peak observed on the single HBC molecule (see Figure 1a). Hence, quantum information on the central dimer bond is not contained within this resonance.

The identified second set $|\psi_l^*\rangle$ of HBC(2) molecular electronic states is composed of at least six Slater determinants built up with a large contribution from LUMO+6. The LUMO+6 ESQC calculated monoelectronic STM image alone reproduces quite well and with the good symmetry the +2.85 V resonance d*I*/d*V* map as shown in Figure 2d,g, although it has not been possible to identify yet the full superposition of its monoelectronic components. As presented in the Figure 3 molecular orbital correlation diagram, the information of the intermonomer chemical bond is not contained in the $|\psi_l^*\rangle$ contributing to this +2.85 V resonance. The d*I*/d*V* measurement at this energy over the central part of the HBC dimer captures mainly the variation of the junction conductance controlled by the LUMO+6 component of this state. LUMO+6 results from a symmetric superposition of high energy single HBC moieties π MO ($|\pi_l^*\rangle$ state in Figure 3) and carries no information on the chemical stability of HBC(2). Its antisymmetric counterpart $|\psi_{l'}^*\rangle$ has also been identified and its monoelectronic ESQC STM image calculated (see Figure 3). The actual antibonding states of

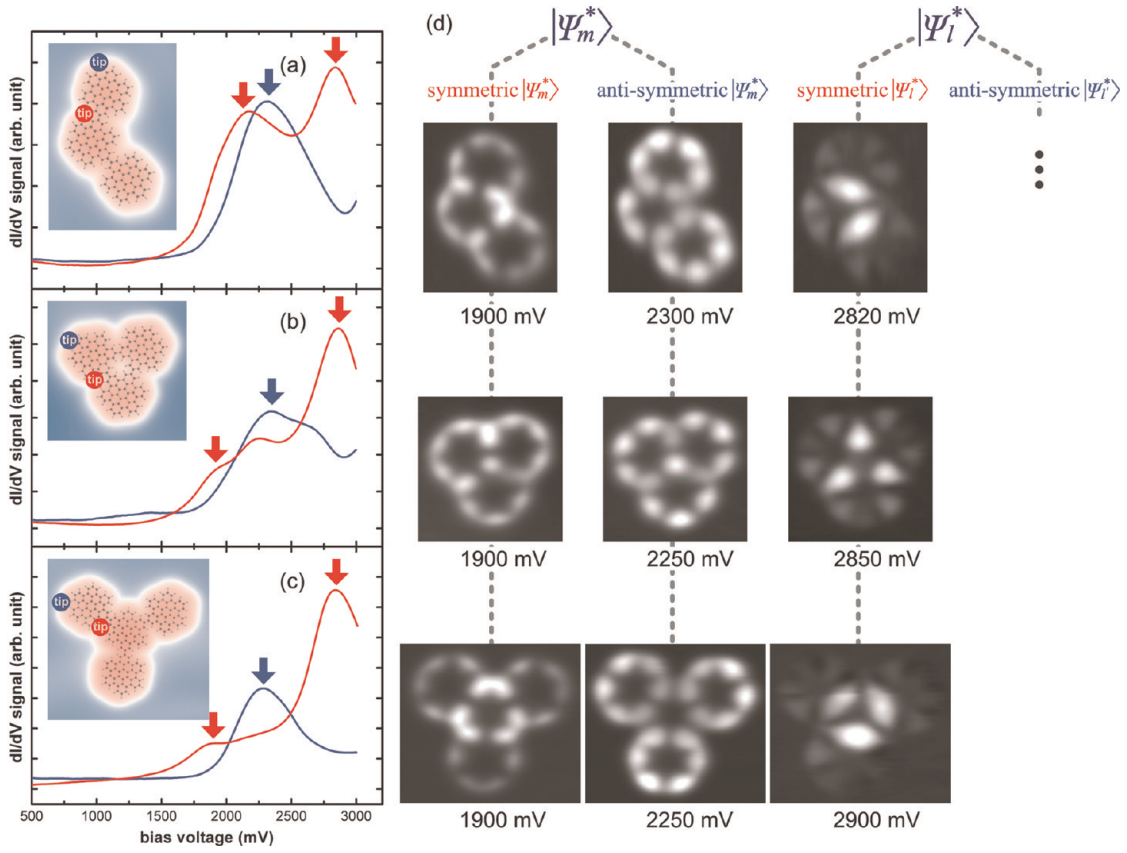

Figure 4. Scanning tunneling spectroscopic data of HBC trimers and tetramer. (a–c) d*I*/d*V* spectra taken at the center between HBC partners (red line) and on the outer edge of oligomers (blue line). Insets show the topographic images of each oligomer and their respective skeleton molecule models. The exact tip locations where each spectrum was measured is indicated by the red and blue dots. (d) d*I*/d*V* maps taken at the peak positions labeled in the spectra. Image sizes are 3.5 nm × 4.8 nm, 4.0 nm × 4.0 nm, and 4.8 nm × 4.3 nm from top row.

the HBC(2) central covalent bond are out of the STM tunnel junction bias voltage range of stability. Following the usual literature nomenclature, the +2.05 and +2.85 V resonances would have been named LUMO and LUMO+1 resonances.[19] According to the LUMO weight on all of the 12 states captured around this +2.05 V resonance, this is almost valid for the LUMO. On the contrary, the +2.85 V resonance cannot be called LUMO+1. It is more appropriate to name it LUMO+6 according to the molecular excited state decomposition table given in Supporting Information and also to the comparison between the experimental and calculated images.

The d*I*/d*V* spectra and maps have also been recorded for larger oligomers made of up to the HBC(4) tetramer, as presented in Figure 4. Interestingly, the excited states of these large molecules combine in the junction conductance to give rise to a small number of resonances. According to the d*I*/d*V* experimental maps, they do not derive from a simple superposition of the corresponding π molecular orbitals conductance map of the HBC partners. There are now at least 18 states contributing to the first two resonances in Figure 4a,b and 24 states in Figure 4c. According to the corresponding STM maps, all of the second column images in Figure 4d are coming from an antisymmetric combination occurring among all of those states, leading to a splitting in two groups and therefore creating two resonances. Attributing the first red resonances to the b_{3u} LUMO and the second one to the b_{1g} LUMO+1 would therefore be incorrect. All of the third red resonances are coming from the symmetric superposition of other high energy π molecular orbitals of the HBC fragments hybridized because of their closed spatial proximity. However, they do not carry information of the intermonomer covalent bonds. Away from these σ central bonds, the recorded spectra are not very perturbed by the bonding. A resonance doublet succeeds to emerge only for the case shown in Figure 4b.

CONCLUSIONS

By a detailed d*I*/d*V* conductance mapping on rather large molecules, we have demonstrated that STM molecular junction d*I*/d*V* resonances cannot be simply attributed to molecular orbitals but to a specific superposition of molecular states created by the molecular junction STM conductance measurement. Our work also demonstrates that the quantum information about a given chemical bond on a molecule oligomer can be carried out by $|\psi_n\rangle$ located far

away in energy from the low-lying molecular states accessible to STM electronic spectroscopy. Resonance identifications commonly practiced in many STM recorded d*I*/d*V* electronic spectra have to now be revisited. This is pointing out the need for developing a complete many-body scattering theory. This theory would have to take into account how the electronic coupling with the tunnel junction electrodes is mixing together all of the multiconfiguration electronic states of the molecule inserted in this junction leading to electronic resonances which are not simply a linear combination of the $|\psi_n\rangle$ resonances. This is very important for the prospect of long-range quantum information transfer through a single molecular wire or to optimize the chemical structure of a single molecule logic gate.

EXPERIMENTAL SECTION

The Au(111) substrate used in these experiments was cleaned using standard sputtering, by Ne ions, and annealing, at 773 K, cycles lasting approximately an hour each. HBC molecules are sublimed from a crucible heated to ~673 K for 2 min with the Au(111) substrate held at ~473 K to facilitate molecular diffusion. Thereafter, the substrate temperature is quickly ramped up to ~600 K and held for a few seconds to induce bonding between the HBC molecules before cooling it down with liquid helium; this postdeposition annealing stage was only used for preparing samples showing binding molecules. We perform all STM experiments using a Createc low-temperature STM operating at a base pressure of at least 8×10^{-11} mbar at 5 K. Tips for scanning and spectroscopic measurements are prepared by electrochemical etching of a 0.25 mm tungsten wire. A detailed description of the synthesis of hexa-*peri*-hexabenzocoronene (HBC) is given elsewhere.[20]

It has been suggested by other research groups that, at certain temperature, molecules could undergo dehydrogenation; likewise, in our experiments, the proposed reaction involves dehydrogenation from one carbon atom of a single HBC molecule, hence forming HBC radicals. Subsequently, the dehydrogenated intermediates diffuse on the substrate surface until they found another neighboring HBC radical resulting in intermolecular colligation forming dimers. The bond formation is thermally assisted since it takes place only after certain temperature threshold is overcome, and samples treated at lower temperatures only show single HBC molecules (see Supporting Information).

Conflict of Interest: The authors declare no competing financial interest.

Acknowledgment. We acknowledge financial support from the Agency of Science, Technology and Research (A*STAR) - the Visiting Investigatorship Program (Phase III): AtomTech Project, the AtMol European Commission integrated project, the German Science Foundation and the German Ministry of Education and Research.

Supporting Information Available: Details of theoretical works and HBC oligomers' preparation process, Tables S1 and S2, Figures S1−S5. This material is available free of charge *via* the Internet at http://pubs.acs.org.

REFERENCES AND NOTES

1. Davidson, E. R. *Reduced Density Matrices in Quantum Chemistry*; Academic Press: New York, 1976.
2. Melmed, A. J.; Muller, E. W. Study of Molecular Patterns in the Field Emission Microscope. *J. Chem. Phys.* **1958**, *29*, 1037–1041.
3. Hashimoto, H. Development of High Resolution Electron Microscopy in Atomic Level and Its Future. *J. Electron Microsc.* **1979**, *28*, S1–S8.
4. Pusching, P.; Berkebile, S.; Fleming, A. J.; Koller, G.; Emtsev, K.; Seyller, T.; Riley, J. D.; Ambrosch-Draxl, C.; Netzer, F. P.; Ramsey, M. G. Reconstruction of Molecular Orbitals Density from Photo-Emission Data. *Science* **2009**, *326*, 702–706.
5. Lippel, P. H.; Wilson, R. J.; Miller, M. D.; Chiang, S. High-Resolution Imaging of Copper-Phthalocyanine by Scanning-Tunneling Microscopy. *Phys. Rev. Lett.* **1989**, *62*, 171–174.
6. Repp, J.; Meyer, G.; Stojkovic, S.; Gourdon, A.; Joachim, C. Molecules on Insulating Films: STM Images of Individual Molecular Orbitals. *Phys. Rev. Lett.* **2005**, *94*, 026803.
7. Soe, W.-H.; Manzano, C.; De Sarkar, A.; Chandrasekhar, N.; Joachim, C. Direct Observation of Molecular Orbitals of Pentacene Physisorbed on Au(111) by Scanning Tunneling Microscope. *Phys. Rev. Lett.* **2009**, *102*, 176102.
8. Gross, L.; Mohn, F.; Moll, N.; Liljeroth, P.; Meyer, G. The Chemical Structure of a Molecule Resolved by Atomic Force Microscopy. *Science* **2009**, *325*, 1110–1114.
9. Guillermet, O.; Gauthier, S.; Joachim, C.; de Mendoza, P.; Lauterbach, T.; Echavarren, A. STM and AFM High Resolution Imaging of Adsorbed Single Decastarphene Molecules. *Chem. Phys. Lett.* **2011**, *511*, 482–485.
10. Villagomez, C.; Zambelli, T.; Gauthier, S.; Gourdon, A.; Barthes, C.; Stojkovic, S.; Joachim, C. A Local View on Hyperconjugation. *Chem. Phys. Lett.* **2007**, *450*, 107–111.
11. Watson, M. D.; Fechtenkotter, A.; Müllen, K. Big is Beautiful: "Aromaticity" Revisited from the Viewpoint of Macromolecular and Supramolecular Benzene Chemistry. *Chem. Rev.* **2001**, *101*, 1267–1300.
12. Sautet, P.; Joachim, C. Calculation of Benzene on Rhodium STM Images. *Chem. Phys. Lett.* **1991**, *185*, 23–30.
13. Hohenberg, P.; Kohn, W. Inhomogeneous Electron Gas. *Phys. Rev.* **1964**, *136*, B864–B871.
14. Rouillé, G.; Steglich, M.; Huisken, F.; Henning, T.; Müllen, K. UV/Visible Spectroscopy of Matrix-Isolated Hexa-Peri-Hexabenzocoronene: Interacting Electronics Sates and Astrophysical Context. *J. Chem. Phys.* **2009**, *131*, 204311.
15. Leoni, T.; Guillermet, O.; Walch, H.; Langlais, V.; Scheuermann, A.; Bonvoisin, J.; Gauthier, S. Controlling the Charge State of a Single Redox Molecular Switch. *Phys. Rev. Lett.* **2011**, *106*, 216103.
16. Jung, T. A.; Schlittler, R. R.; Gimzewski, J. K.; Tang, H.; Joachim, C. Room Temperature Assembly of Nanostructure by Manipulating Individual Molecule. *Science* **1996**, *271*, 181–184.
17. Treier, M.; Pignedoli, C. A.; Laino, T.; Rieger, R.; Müllen, K.; Passerone, D.; Fasel, R. Surface-Assisted Cyclodehydrogenation Provides a Synthetic Route towards Easily Processable and Chemically Tailored Nanographenes. *Nat. Chem.* **2011**, *3*, 61–67.
18. Stewart, J. J. P. Optimization of Parameters for Semi-Empirical Methods V: Modification of NNDO Approximations and Applications to 70 Elements. *J. Mol. Model.* **2007**, *13*, 1173–1213.
19. Repp, J.; Liljeroth, P.; Meyer, G. Coherent Electron−Nuclear Coupling in Oligothiophene Molecular Wires. *Nat. Phys.* **2010**, *6*, 975–979.
20. Müller, M.; Kübel, C.; Müllen, K. Giant Polycyclic Aromatic Hydrocarbons. *Chem.—Eur. J.* **1998**, *4*, 2099–2109.